Published in final edited form as:
Apoptosis. 2008 May ; 13(5): 621–633. doi:10.1007/s10495-008-0196-7.

Differential patterns of peroxynitrite mediated apoptosis in proximal tubular epithelial cells following ATP depletion recovery

Vani Nilakantan[1,2], **Huanling Liang**[1], **Cheryl J. Maenpaa**[1,2], and **Christopher P. Johnson**[1,2,3]

1 *Division of Transplant Surgery, Medical College of Wisconsin, Milwaukee, WI 53226, USA*

2 *Kidney Disease Center, Medical College of Wisconsin, H4135, 8701 Watertown Plank Road, Milwaukee, WI 53226, USA*

3 *VA Medical Center, Medical College of Wisconsin, Milwaukee, WI 53226, USA*

Abstract

Ischemia-reperfusion injury (IRI) is characterized by ATP depletion in the ischemic phase, followed by a rapid increase in reactive oxygen species, including peroxynitrite in the reperfusion phase. In this study, we examined the role of peroxynitrite on cytotoxicity and apoptosis in an in vitro model of ATP depletion-recovery. Porcine proximal tubular epithelial (LLC-PK$_1$) cells were ATP depleted for either 2 h (2/2) or 4 h (4/2) followed by recovery in serum free medium for 2 h. A subset of cells was treated with 100 μM of the peroxynitrite scavenger, iron (III) tetrakis (N-methyl-4′pyridyl) porphyrin pentachloride (FeTMPyP) 30 min prior to and during treatment/recovery. Treatment with FeTMPyP reduced cytotoxicity and superoxide levels at both the 2/2 and 4/2 time points, however FeTMPyP decreased nitric oxide only at the 2/2 time point. FeTMPyP also partially blocked caspase-3 and caspase-8 activation at both 2/2 and 4/2 time points. At the 4/2 time point, FeTMPyP also partially inhibited the ATP depletion mediated increase in tumor necrosis factor alpha (TNF-α) and decreased Bax and FasL gene expression. These data show that peroxynitrite induces apoptosis by activation of multiple pathways depending on length and severity of insult following ATP depletion-recovery.

Keywords

Ischemia-reperfusion; Superoxide; Peroxynitrite; ATP depletion; Proximal tubular epithelial cells; FeTMPyP; Apoptosis; Caspase-3; Bcl-2

Introduction

Ischemia-reperfusion injury (IRI) is a major cause of acute renal failure and graft dysfunction following transplantation. During the ischemic phase of IRI, there is a depletion of ATP [1–3] followed a rapid increase in reactive oxygen species (ROS) including superoxide ($O_2^{\bullet -}$) during reperfusion. Concurrently, ischemia induces nitric oxide synthase (iNOS) in renal tubular epithelial cells generating nitric oxide (NO) [4]. $O_2^{\bullet -}$ readily combines with NO at diffusion controlled rates to form the highly reactive and potently nitrating species, peroxynitrite [5–7]. In some biological systems, the rate of peroxynitrite production can be as high as 50–100 μM [8], although the steady state concentrations are in the nanomolar range. Peroxynitrite readily reacts with proteins to form 3-nitrotyrosine, tyrosine dimers or oxidation of thiol groups [9–12] which can either lead to inactivation or enhanced degradation [13–16]

e-mail: vnilakan@mcw.edu.

of the proteins. Further, peroxynitrite can also cause adduct formation, oxidation and strand breaks in DNA [16–18].

Reactive oxygen mediated damage to proximal tubular epithelial cells has been demonstrated in various models of chemically induced hypoxia [19–21]. Using pyruvate, a hydrogen peroxide scavenger and exogenous superoxide dismutase, Hagar et al. [22] have shown that early apoptotic signaling in chemical hypoxia is mediated by free radicals. Proximal tubular cells are particularly more susceptible to apoptosis due to IR and ATP depletion [23–25] due to the fact that this region is marginally oxygenated and lacks the ability to generate significant amounts of ATP via glycolysis [26] and primarily depends on oxidative phosphorylation for energy production. We have also previously shown that ROS mediate apoptosis in proximal tubular epithelial cells (LLC-PK_1) cells by promoting the release of cytochrome *c* from the mitochondria at early time points after ATP depletion and by activating tumor necrosis factor alpha (TNF-α) mediated apoptosis in the later stages of ATP depletion [27].

There is evidence that reactive nitrogen species such as peroxynitrite also impair mitochondrial function by inhibiting respiration and inactivating Complex I [28,29]. Additionally, the tyrosine nitration and inactivation of manganese superoxide dismutase (MnSOD) [9,11] and cytochrome c [30,31] by peroxynitrite can amplify mitochondrial injury and lead to pro-apoptotic signaling. Further, increased peroxynitrite can activate poly-ADP ribosyl synthetase (PARP) [32], resulting in depletion of ATP and NAD^+ stores and necrotic cell death.

Several synthetic metalloporphyrins have been developed as potent peroxynitrite decomposition catalysts, including 5,10,15,20-tetrakis (2,4′,6′-trimethyl-3′5′-disulphonatopheyl) porphyrinato iron III (7^-) (FeTMPS) and 5,10,15,20-tetrakis (N-methyl-4′-pyridyl) porphyrinato iron III (5^+) (FeTMPyP) [33,34]. Cuzzocrea et al. (2000) have shown that FeTMPS was effective in reducing lipid peroxidation and limiting IRI in the bowel in a model of splanchnic artery occlusion [35]. FeTMPyP has also been used successfully in cerebral, intestinal, and myocardial IRI [36–38]. In these models of injury, FeTMPyP blocks neutrophil infiltration, PMN accumulation and lipid peroxidation. Despite these studies, however, it is still not clear whether renal tubular epithelial cells are also susceptible to peroxynitrite induced damage in IRI. Further, the signaling pathways (mitochondrial or receptor) that lead to apoptosis due to increased peroxynitrite formation in renal IRI are not completely understood. In order to address these questions, in this study, we used ATP depletion-recovery in porcine proximal tubular epithelial cells (LLC-PK_1) to simulate in vivo renal IRI and examined the efficacy of FeTMPyP on inhibition of cytotoxicity, ROS and apoptosis. We also determined whether extrinsic or intrinsic pathways of apoptosis are involved in peroxynitrite mediated cell death following ATP depletion-recovery.

Materials and methods

Materials

Porcine renal proximal tubular epithelial cells (LLC-PK_1) were purchased from American Type Culture Collection (Rockville, MD). Growth medium (α-MEM), Dulbecco's PBS (DPBS), fetal bovine serum (FBS), penicillin-streptomycin with L-glutamine, 0.25% Trypsin-EDTA and dihydroethidium were obtained from GIBCO/Invitrogen (Carlsbad, CA). 5,10,15,20-tetrakis (N-methyl-4′-pyridyl) porphyrinato iron III (5^+) (FeTMPyP) was purchased from Axxora (San Diego, CA). Antimycin-A and *n*-butanol were from Sigma (St. Louis, MO). RIPA lysis buffer was from Upstate Biotechnology (Lake Placid, NY). Laemmli sample buffer was from Bio-Rad (Hercules, CA).

Experimental protocols

LLC-PK_1 (ATCC Rockville, MD) cells were grown in α-MEM containing 10% FBS, 100 U/ml penicillin, 100 μg/ml streptomycin, and 290 μg/ml L-glutamine at 37°C in a 5% CO_2/95% air humidified incubator. Cells were plated at $5 * 10^5$ the day prior to the experiment. On the day of experiment, cells were washed with DPBS and incubated with pre-warmed serum free α-MEM 30 min prior to ATP-depletion. ATP depletion was induced by substrate deprivation (in injury media, IM) and the addition of 0.1 μM antimycin A, a complex III inhibitor for either 2 or 4 h. The injury media (IM) consisted of (in mM): 1X MEM vitamin solution (Invitrogen, Carlsbad, CA), 26 $NaHCO_3$, 5.4 KCl, 116 NaCl, 0.9 $NaH_2PO_4 \cdot 2H_2O$, 0.8 $MgSO_4 \cdot 7H_2O$, 1.8 $CaCl_2 \cdot 2H_2O$, and 0.0001 lipoic acid (Sigma, St. Louis, MO). To maintain osmolarity, 5.5 M of the non-metabolizable form of glucose, L-glucose, was added. Following ATP depletion, cells were recovered in serum-free α-MEM for an additional period of 2 h. The recovery media was serum-free α-MEM with 100 U/ml penicillin and 100 μg/ml streptomycin (Invitrogen, Carlsbad, CA). Control cells were grown in parallel and underwent equivalent washes and incubated in serum free α-MEM throughout experiment. A subset of cells received 100 μM of the peroxynitrite decomposition catalyst, FeTMPyP 30 min prior to and during treatment/recovery. At the end of the 2 h recovery, cells were harvested and lysed in RIPA lysis buffer with the addition of protease inhibitors. Protein concentration was measured using a protein assay kit from Bio-Rad (Hercules, CA). Media was also collected and stored at 4°C following ATP depletion and recovery for analysis of LDH release and NO measurements.

LDH measurements

Cytotoxicity, as determined by LDH release, was measured in medium using a commercially available kit (Diagnostic Chemicals, Oxford, CT) on the same day of harvest. LDH activity was normalized to protein levels and is expressed as mU/mg protein.

NO levels

NO levels were measured in the media using the Seivers NO analyzer (Seivers) with sodium nitrate as standard ranging from 3–100 μM. Briefly, media was filtered using Microcon YM-10 filters (Millipore, Billerica, MA) by centrifugation at 14,000 g for 30 min. Ten μL of the filtrate was injected into the NO analyzer and the peak area was quantified and integrated.

Lucigenin-enhanced chemiluminescence

Lucigenin-enhanced chemiluminescence was measured as previously described [39,40]. Briefly, 10 μM lucigenin was added to 1 ml of harvested media or cell-free α-MEM. Lucigenin-enhanced chemiluminescence was measured for 10 s in a luminometer (Berthold Instruments, Autolomat LB 953, Bad Wilblad, Germany). Cell-free α-MEM was read to calculate background luminescence and subtracted from each value. Reactive oxygen production was normalized to protein levels and reported as relative light units emitted (RLU)/min/mg protein.

DHE fluorescence

DHE staining was used for qualitative analysis of intra-cellular $O_2^{\bullet -}$ production. Twenty minutes prior to the end of the 2 h recovery following 2 h ATP depletion, cells were loaded with 10 μM hydroethidine (HE). Cells were incubated with HE in the dark for a period of 15 min and washed 2X with DPBS to remove excess background staining. Cells were then immediately scanned for $O_2^{\bullet -}$ using an Olympus IX50 inverted microscope equipped with rhodamine filter settings.

Apoptosis measurement

Apoptosis was evaluated by flow cytometry via Annexin V and propidium iodide staining according to manufacturer's instructions using flow cytometry (BD Pharmingen, Franklin Lakes, NJ). Annexin V positive cells were classified as apoptotic. Analyses were performed using FACS Calibur flow cytometer (BD, San Jose, CA).

For microscopic visualization, cells were grown on coverslips (diameter 22 mm) coated with poly-L-lysine (Sigma, St. Louis MO). After 2–2 h and 4–2 h ATP depletion with or without FeTMPyP treatment, coverslips were removed from the culture dish and washed with phosphate buffered saline (PBS, pH 7.4), then stained with propidium iodide (5 μg/ml) and Annexin V-FITC (5 μg/ml) (BD Bioscience Pharmingen) in 1x Binding buffer for 15 min at room temperature in the dark. After washing with PBS, the coverslips were mounted on glass slides using Gel/mount (Electron Microscopy Science) and imaged under Nikon fluorescence microscopy.

Caspase-3 and caspase-8 activities in cell extracts were determined by using commercially available colorimetric kits (Chemicon, Temecula, CA) as per manufacturer's instructions. Caspase activity was expressed in μM/min/mg protein. In addition, Western Blotting was performed for caspase-3 as described below (Western Blotting section).

TNF-α measurement

The quantitative determination of tumor necrosis factor alpha (TNF-α) in cell extracts was attained using a commercially available quantitative sandwich ELISA kit (R&D Systems, Minneapolis, MN) per manufacturer's instructions. TNF-α concentration was expressed in pg/mg protein.

Western blots

Protein expression of iNOS, nitrotyrosine, caspase-3, Fas, Fas Ligand (FasL), Bcl-2 and GAPDH was determined via Western blot analysis. Briefly, 20 μg of cellular protein was separated by 12% SDS-polyacrylamide gel electrophoresis and transferred to nitrocellulose membrane for 1.5 h at 4°C. All proteins, except for Bcl-2 were blocked in LiCor blocking buffer (Lincoln, NE) and incubated with one of the following: mouse anti-nitrotyrosine (1:1000, Upstate Biotechnology, Bellerica, MA), rabbit anti-caspase-3 (1:1000, Cell Signaling, Boston, MA), mouse anti-Fas (1:2000, BD Transduction Laboratories, San Jose, CA), rabbit anti-FasL (1:200, Santa Cruz Biotechnology, Santa Cruz, CA), anti-Bax (1:500, Santa Cruz Biotechnology, CA) or mouse anti-GAPDH (1:2000, Chemicon, Temecula, CA), overnight at 4°C. The membrane was then incubated with IRDye infared secondary antibodies (anti-mouse IgG and anti-rabbit IgG, 1:10,000, LiCor, Lincoln, NE) for 1 h at room temperature and visualized with the Odyssey Infared Imaging System (LiCor, Lincoln, NE). For Bcl-2 the membrane was blocked with TBS-0.05% Tween-20 containing 5% milk for 1 h at room temperature. The membrane was incubated with mouse anti-Bcl-2 (1:1000, Santa Cruz Biotechnology, Santa Cruz, CA) overnight at 4°C and visualized with goat anti-mouse IgG HRP (1:10,000, 1 h, room temperature, Bio-Rad, Hercules, CA) and enhanced chemiluminescence (GE Healthcare, Piscat-away, NJ). Densitometry was performed on NIH Image J image analysis ij134 software and proteins were normalized to GAPDH.

Statistical analysis

All values are expressed as means ± standard error of the mean. Statistical analysis was performed by one-way ANOVA, followed by Newman–Keuls multiple comparison test. *P* values lower than 0.05 were considered statistically significant.

Results

In vitro model of ATP depletion-recovery

We used a widely used in vitro model of ATP depletion-recovery of a porcine proximal tubular epithelial cell line (LLC-PK_1) to simulate in vivo renal IRI [19,41]. ATP depletion-recovery was achieved by substrate and amino acid deprivation in combination with a low dose of antimycin A (0.1 μM) for either 2 or 4 h followed by recovery in serum free media for another 2 h (time points 2/2 and 4/2 respectively).

To validate our model of ATP depletion, in preliminary experiments we measured ATP levels at the 2/2 time point of ATP depletion-recovery. ATP levels ranged from 95 pmol/μg protein for 1×10^4 cells to 115 pmol/μg protein for 2×10^4 cells. This was well within the reported range of ATP levels of normal resting LLC-PK1 cells [1]. We found that ATP was depleted by 80% compared to control cells at the 2/2 time point and by 90% at time point 4/2 (data not shown). Further, treatment with 100 μM of FeTMPyP had no effect on ATP levels (data not shown).

FeTMPyP decreases cytotoxicity following ATP depletion-recovery

There was an increase in LDH release in LLC-PK_1 cells following ATP depletion and recovery at both the 2/2 time point (serum free, uninjured (control) 3.35 ± 0.09 mU/mg protein, ATP depletion-recovery (IM) 6.63 ± 0.42 mU/mg protein, $P < 0.01$, $n = 3–9$) and the 4/2 time point (control 4.08 ± 0.64 mU/mg protein, IM 6.67 ± 0.99 mU/mg protein, $P < 0.01$, $n = 7–8$) (Fig. 1). Treatment with FeTMPyP was effective in significantly lowering cytotoxicity ($P < 0.01$ FeTMPyP vs. IM) at both the 2/2 (3.25 ± 0.78 mU/mg protein, $n = 4$) and 4/2 time points (3.54 ± 0.78 mU/mg protein, $n = 7$) (Fig. 1a).

To ensure that FeTMPyP did not have any effect on the cells by itself, we did a control experiment in which we treated LLC-Pk_1 cells with 100 μM FeTMPyP for both 2 h of ATP depletion-2 h recovery (2/2) and 4 h ATP depletion-2 h recovery (4/2). As shown in Fig. 1b, FeTMPyP treatment by itself had no effect on LDH release in the cells, indicating that there was no cytotoxic effect of the drug by itself.

FeTMPyP decreases NO levels only at the early time point following ATP depletion-recovery

In order to determine whether use of the peroxynitrite decomposition catalyst also decreased NO levels, we measured nitrate/nitrite in the media and iNOS protein expression in the cell extracts of serum free, IM and FeTMPyP treated LLC-PK_1 cells at the 2/2 and 4/2 time points.

There was minimal change in iNOS protein levels at the early time point of ATP depletion (Fig. 2a, upper panel) and a variable and slight increase in iNOS at the later time point (Fig. 2a, lower panel) with none of the groups being statistically significant from each other. FeTMPYP did not have a significant effect on iNOS protein levels at either time point (Fig. 2).

NO levels were unchanged between serum free controls and IM groups at both the 2/2 (control 3.27 ± 0.23 μM, IM 3.68 ± 0.22 μM, $n = 4–7$) and 4/2 time points (control 2.69 ± 0.34 μM, IM 2.53 ± 0.25 μM, $n = 4–5$) (Fig. 2b). Interestingly, FeTMPyP decreased NO levels (FeTMPyP 2.11 ± 0.16 μM, $n = 4$) at the early (2/2) time point following ATP depletion-recovery (Fig. 2b) without affecting iNOS expression (Fig. 2a). At the later time point of ATP depletion-recovery (4/2), FeTMPyP had no effect on NO levels (FeTMPyP 2.62 ± 0.03 μM, $n = 5$) (Fig. 2).

FeTMPyP decreases ROS following ATP depletion-recovery

In order to determine whether FeTMPyP decreased ROS, we measured reactive oxygen in the media by lucigenin enhanced chemiluminescence and intracellular superoxide by DHE fluorescent microscopic imaging in the cells.

Lucigenin enhanced chemiluminescence was increased by ATP-depletion at both 2/2 (serum free controls 580 ± 30.85 RLU/min/mg protein, IM 874 ± 78.59 RLU/min/mg protein, $P < 0.001$ IM vs. control $n = 6$) and 4/2 (serum free controls 532 ± 48.04 RLU/min/mg protein, IM 962 ± 205.65 RLU/min/mg protein, $P < 0.001$ IM vs. controls, $n = 3$) time points (Fig. 3a). Treatment with FeTMPyP resulted in a dramatic decrease in lucigenin-enhanced chemiluminescence at both time points (2/2: 327 ± 29.04 RLU/min/mg protein, $P < 0.01$ FeTMPyP vs. IM, $n = 6$; 4/2: 322 ± 14.23 RLU/min/mg protein, $P < 0.05$, FeTMPyP vs. IM, $n = 3$) (Fig. 3a).

DHE fluorescent microscopic imaging following ATP depletion-recovery at time point 2/2 showed that there was increased DHE fluorescence in injured cells compared to serum free controls, indicating that there was increased intracellular superoxide production at this early time point of injury (Fig. 3b). Treatment with FeTMPyP scavenged the superoxide since the staining in FeTMPyP treated cells was similar to control levels (Fig. 3b).

Effect of FeTMPyP on nitrotyrosine levels following ATP depletion-recovery

We next examined the effect of FeTMPyP on nitrotyrosine formation, a marker for peroxynitrite formation, in our model of injury. Surprisingly, there was not any increase in nitrotyrosine levels as detected by Western Blotting techniques in cells that were subject to ATP depletion-recovery (Fig. 3c) at both the 2/2 and 4/2 time points. Nevertheless, FeTMPyP did decrease nitrotyrosine levels moderately after 2 of ATP depletion and a more dramatic decrease after 4 h of ATP depletion (Fig. 3c).

FeTMPyP partially attenuates early apoptotic signaling following ATP depletion-recovery

We used several methods to determine apoptosis. We performed Annexin V/Propidium Iodide staining followed by flow cytometry to determine early apoptotic signaling and necrosis. As shown in Fig. 4a, ATP depletion-recovery of the LLC-PK_1 cells increased early apoptotic signaling from 9.63% (serum free control) to 21.01% (IM) at the early time point of 2/2. Treatment with FeTMPyP had a very minor impact on early apoptotic signaling and reduced it from 21.01% (IM) to 18.65% (FeTMPyP). At the later time point of 4/2, IM treatment increased early apoptotic signaling from 5.98% (serum free control) to 23.31% (IM). FeTMPyP partially attenuated apoptosis at this time point to 16.60%. We also performed annexin V staining followed by microscopy to confirm this result (Fig. 4b, lower (AV) panels of 2/2 and 4/2 images). There was a slight increase in Annexin V staining at time point 2/2 and a more substantial increase at time point 4/2 indicating increased apoptosis. FeTMPyP was effective in partially blocking the Annexin V staining at both time points.

Surprisingly, we could not detect increased propidium iodide staining after either the early or late time points of injury by this method. To further examine whether ATP depletion-recovery increased cell death by necrosis, we evaluated necrosis by propidium iodide staining followed by microscopic imaging in serum free, IM and FeTMPyP treated cells at both the early (2 h/2 h) and the later time points (4 h/2 h). As shown in Fig. 4b, there was moderate increase in propidium iodide staining (as indicated by punctate bright red staining, upper panels of Fig. 4b) at the early time point and a more pronounced increase after 4 h/2 h ATP depletion and recovery. This increase was only partially attenuated by the addition of FeTMPyP to the IM (Fig. 4b).

Effect of FeTMPyP on activation of caspase-3 following ATP depletion-recovery

We further examined apoptosis by measuring the activity of casapse-3, the downstream effector protease of apoptosis. The activity of caspase-3 was increased from 3.26 ± 0.78 μM/min/mg protein (serum free controls) to 20.67 ± 0.91 μM/min/mg protein (IM) at the early time point (2/2) following ATP depletion-recovery (Fig. 5a, $P < 0.001$ IM vs. serum free, $n = 3$). Addition of FeT-MPyP to the IM resulted in a significant decrease in caspase-3 activation (Fig. 5a, FeTMPyP 7.92 ± 0.64 μM/min/mg protein, $P < 0.01$ vs. IM, $n = 3$).

At the later time point (4/2), caspase-3 activity was increased from 2.83 ± 0.84 μM/min/mg protein (serum free) to 38.75 ± 3.88 μM/min/mg protein (IM) (Fig. 5a, $P < 0.01$ IM vs. serum free, $n = 3$). Surprisingly, treatment with FeTMPyP at this time point did not inhibit the activation of caspase-3 and actually increased it mildly (Fig. 5a, FeTMPyP 51.33 ± 1.33 μM/min/mg protein).

Western Blotting at this time point indicated the appearance of the activated cleaved caspase-3 band at about 17 KDa (Fig. 5b) in the ATP depleted cells. Interestingly, in contrast to the activity assay, FeTMPyP significantly decreased the intensity of the cleaved caspase-3 band (Fig. 5b).

FeTMPyP inhibits caspase-8 activation in both the early and late phases of ATP depletion-recovery

We next determined whether the extrinsic pathway of apoptosis was activated in our model of injury and if peroxynitrite played a role in activating this pathway. We did this by first measuring caspase-8, a protease that is recruited and activated by the Fas and TNF death domains. Caspase-8 was activated significantly at the 2/2 time point in the ATP depleted cells compared to serum free controls (Fig. 5c, control 2.14 ± 0.76 μM/min/mg protein, IM 10.04 ± 1.2 μM/min/mg protein, $P < 0.05$ IM vs. control, $n = 3$). Treatment with FeTMPyP significantly decreased caspase-8 to 2.65 ± 0.24 μM/min/mg protein, $P < 0.05$ FeTMPyP vs. IM). At the 4/2 time point, caspase-8 activity increased from 3.05 ± 0.56 μM/min/mg protein in serum free controls to 26.14 ± 1.57 μmol/min/mg protein in the IM samples (Fig. 5c, $P < 0.001$ IM vs. control, $n = 3$). Thus, caspase-8 activation was more than doubled in the later phases of injury. Addition of FeTMPyP decreased caspase-8 activation by half i.e. to 10.55 ± 0.55 μM/min/mg protein (Fig. 5c, $P < 0.01$ FeTMPyP vs. IM, $n = 3$)

Effect of FeTMPyP on the receptor mediated pathway of apoptosis following ATP depletion-recovery

To further delineate the pathways that lead to caspase-8 activation, namely TNF/Fas mediated pathways of apoptosis, we evaluated TNF-α levels and expression of Fas/FasLigand (FasL) in serum free, IM and FeTMPyP treated cells.

TNF-α levels were measured in the cell extracts using ELISA in serum free, IM and FeTMPyP treated cells. As shown in Fig. 6a, there was a significant increase in TNF-α levels in ATP depleted cells at the 2/2 time point (serum free control 0.88 ± 0.02 pg/mg protein, IM 1.52 ± 0.22 pg/mg protein, $P < 0.05$ control vs. IM, $n = 3$). Treatment with FeTMPyP did not significantly decrease TNF-α levels (1.28 ± 0.04 pg/mg protein) (Fig. 6a). At the later time point of 4/2, TNF-α was dramatically increased (Fig. 6a, control 0.89 ± 0.04 pg/mg protein, IM 2.62 ± 0.17 pg/mg protein, $P < 0.01$ serum free vs. IM, $n = 3$). There was a decrease in TNF-α levels in the FeTMPyP treated cells (Fig. 6a, FeTMPyP 2.02 ± 0.03, $P < 0.05$ FeTMPyP vs. IM, $n = 3$).

There was minimal change in FasL expression in LLC-PK_1 cells following ATP depletion recovery at the 2/2 time point compared to serum free controls (Fig. 6b, left panel). FeTMPyP

did not have a significant effect on Fas or FasL expression at this early time point (Fig. 6b, left panel). Following longer durations of ATP depletion-recovery i.e. at the 4/2 time point, although there was no change in Fas gene expression between serum free and IM groups (Fig. 6b, right panel), there was a small increase in FasL gene expression in ATP depleted cells (IM) compared to serum free controls (Fig. 6b, right panel). FeTMPyP treatment decreased FasL gene expression to below control levels (Fig. 6b, right panel).

Effect of FeTMPyP on the mitochondrial pathway of apoptosis in LLC-PK$_1$ cells following ATP depletion-recovery

We wanted to finally determine if peroxynitrite activated the mitochondrial pathway of apoptosis in our model of injury. We measured protein levels of the anti-apoptotic protein Bcl-2 which prevents the permeabilization of the mitochondrial membrane thereby preventing the release of cytochrome *c* and the pro-apoptotic protein Bax, which promotes the release of cytochrome *c* into the cytosol. Interestingly, there was no change in Bcl-2 protein levels in the treatment groups at the 2/2 (Fig. 7, left panel). Bax expression also did not change at the early time point of 2/2 between any of the groups (Fig. 7, left panel). At the later time point of 4/2, there was an increase in Bcl-2 protein following ATP depletion-recovery, although Bax protein levels did not change between serum free controls and IM treated cells (Fig. 7, right panel). FeTMPyP treatment decreased both Bcl-2 and Bax protein levels compared to the IM group (Fig. 7, right panel).

Discussion

In this study, we tested the efficacy of the peroxynitrite decomposition catalyst, FeTMPyP in limiting cytotoxicity and apoptosis in proximal tubular epithelial cells (LLC-PK$_1$) following ATP depletion-recovery. This model of chemically induced hypoxia has been used extensively by us and other investigators to simulate renal IRI in vitro [19,41]. Whereas other investigators have used differing amounts of ATP to achieve graded injury [41], we have used short (2 h) and long (4 h) times of ATP depletion to achieve graded injury. The main results of the study were as follows: (1) FeTMPyP was effective in attenuating cytotoxicity after both short (time point 2/2) and long (time point 4/2) durations of ATP depletion-recovery (2) FeTMPyP decreased reactive oxygen at both time points but decreased NO levels only at the early time point of ATP depletion (2/2) (3) FeTMPyP inhibited activation of caspase-3 and inhibited casaspe-8 at both time points (4) FeTMPyP had a partial effect on decreasing FasL and TNF-α levels following longer durations of injury (4/2) and further significantly blocked activation of Bax at this time point.

We found that exposing the LLC-PK$_1$ cells to IM for as short as 2 h resulted in a massive decrease in ATP levels (80%) which was further decreased to 90% of serum free controls after 4 h of ATP depletion. ATP levels remained low throughout the recovery period and treatment with FeTMPyP did not significantly increase ATP levels. Although this was surprising, this result correlated with our previous studies in which the cell permeable SOD mimetic, MnTMPyP significantly attenuated cytotoxicity without affecting ATP levels [27].

There was a significant increase in cytotoxicity in LLC-PK$_1$ cells following both 2/2 and 4/2 h of ATP depletion-recovery. Treatment with FeTMPyP decreased LDH release back to levels in control (serum free) cells indicating that peroxynitrite plays a significant role in proximal tubular epithelial cell damage following ATP depletion-recovery. There is ample evidence that superoxide can readily react with NO to form the highly potent and reactive peroxynitrite radical [42–44] which can modify DNA and proteins resulting in cellular damage. Although we have previously shown that superoxide is one of the mediators of cell death in this model of injury [27], it is possible that there is an increase in the production of peroxynitrite following

ATP depletion-recovery which is also partially responsible for the damage to the proximal tubular epithelial cells.

Since there are reports reporting that FeTMPyP provides protection against intestinal IRI at least partially by decreasing systemic NO production [37], we measured nitrate/nitrite levels in control, IM and FeTMPyP treated LLC-PK_1 cells. Interestingly, FeTMPYP decreased NO levels to the levels found in serum free control cells at the 2/2 time point, but had no effect on NO at the later time point of 4/2. It is not yet clear why FeTMPyP had a biphasic effect on NO levels in this model of injury, although it is possible that FeTMPyP exerts its effects by both attenuating NO levels at the early time points and by the decomposition of peroxynitrite and in an NO-independent manner at the later time points of injury. Similarly, there is a recent report indicating that FeTMPyP decreases apoptosis without affecting NO production [38] in a model of myocardial IRI, providing evidence that peroxynitrite but not NO itself is responsible for the myocardial ischemic nitrative stress.

There is accumulating evidence that FeTMPyP not only acts as a peroxynitrite scavenger but can also catalytically scavenge superoxide anion thereby decreasing overall oxidative stress [34,36,45]. We tested this action of FeTMPyP to scavenge superoxide following ATP depletion-recovery by measuring ROS levels by lucigenin enhanced chemiluminescence and intracellular production of superoxide by DHE staining. In our model, there was an increase in ROS levels following ATP depletion-recovery; FeTMPyP was effective in decreasing ROS levels at both the early and late time points following ATP depletion-recovery. Thus, this indicates that FeTMPyP has multiple modes of action, including decreasing ROS levels and does not act by peroxynitrite decomposition alone.

Interestingly, when we evaluated peroxynitrite formation by Western blot we did not detect an increase in nitrotyrosine formation at either time point (see Fig. 3c). It is not really clear yet why we could not detect increased nitrotyrosine, although it could be related to limited detection capability in this particular technique. Nevertheless, FeTMPyP did decrease nitrotyrosine levels moderately at the 2/2 time point and more significantly at the 4/2 time point, indicating that it was effective in reducing peroxynitrite formation. It is well established that small amounts of NO can react very fast with superoxide to form peroxynitrite at diffusion limited rates. In fact, NO can out compete superoxide dismutase for its substrate, superoxide. This would indicate that basal or constitutive levels of NO are sufficient to form peroxynitrite when there is excess superoxide formation. In our studies, we did find increased superoxide formation by lucigenin and DHE fluorescent techniques; this was also decreased by FeTMPyP. It is possible that FeTMPyP acts both by decreasing peroxynitrite as well as behaving as a superoxide scavenger thereby decreasing overall oxidative stress in the cells.

We next tested whether FeTMPyP had a significant impact on apoptosis. We performed Annexin V/propidium iodide based flow cytometry to determine apoptosis. At both time points, there was an increase in early apoptotic signaling. Necrosis was also increased as measured by propidium iodide staining followed by microscopy with more pronounced staining at the later stages of injury. This is similar to our previous study in which we had determined that ATP depletion for a period of 6 h leads to necrosis but shorter durations of injury lead to apoptotic signaling [27]. FeTMPyP decreased apoptosis slightly at the earlier time point and had a more significant impact on apoptosis at the 4/2 time point. A recent investigation by Tiwari et al. (2006) [46] suggests that proximal tubular cells are more sensitive to superoxide rather than NO mediated apoptosis in a model of LPS induced injury. From our model, it however seems more likely that multiple radicals including superoxide, NO and peroxynitrite play a role in exacerbating cellular damage.

In conjunction with flow cytometry, we also determined apoptosis by measuring the activation of caspase-3, a downstream effector protease upon which multiple pathways converge. A number of studies have shown that increased ROS and RNS play an important role in the activation of caspase-3 in ischemia-reperfusion [47–49]. As expected, in our model of injury, there was activation of caspase-3 in IM treated cells vs. serum free controls, and FeTMPyP significantly blocked this activation. Surprisingly, however, by this method, FeTMPyP did not block caspase-3 activation following the longer duration of ATP depletion-recovery and in fact increased the caspase-3 activity slightly, although there was a decrease in the activated caspase-3 band by Western Blotting at this time point. The reasons for this discrepancy in caspase-3 at this later time point are not really clear though there could be two reasons for this. First, it is possible that caspase-3 activity assay may be detecting non-specific protease activity that occurs due to multiple freeze-thaw of the samples. Indeed, we have found that there is usually about 25% non-caspase-3 specific protease activity in samples that have undergone multiple freeze-thaw cycles (unpublished observations). Secondly, it is possible that the inability of FeTMPyP to block caspase-3 activation at later time points of injury could be due to induction of apoptosis in a caspase-3 independent manner following longer durations of injury. It has been shown that caspase-7, another effector protease of apoptosis, although structurally related to caspase-3, has substrates distinct from caspase-3 and has a different subcellular localization [50]. Further, treatment of proximal tubular epithelial cells with high dose (0.5 mM) of NO donors activates both caspase-3 and caspase-7 [51]. Neuroblastoma cells that are treated with actimomycin D also display increased ROS and activation of caspase-7 but not caspase-3 [52]. Based on these reports, it is possible that following ATP depletion, peroxynitrite may have a dual mode of action; i.e. induction of apoptosis by activation of both caspase-3 and caspase-7. FeTMPyP was also effective in blocking caspase-8 activation at both the early (2/2) and late (4/2) time points of ATP depletion-recovery. This confirmed to us that peroxynitrite was activating a pathway other than caspase-3 at the later time point of injury. Direct recruitment of caspase-8 can occur by extrinsic signals that activate the death receptors: TNF receptor-associated death domain (TRADD) and the Fas-associated death domain (FADD) [53–55]. These receptors are activated by the ligands, TNF-α and Fasligand (FasL). Interestingly, in our model of injury there was an increase in TNF-α levels after both the early and late phases of injury but FeTMPyP decreased TNF-α levels only at the late time point of 4/2. Although there was no change in Fas expression at this time point, there was a small increase in FasL expression that was partially blocked by FeTMPyP. This indicated that caspase-8 activation by peroxynitrite in our model of injury is at least partially dependant on TNF-α and FasL suggesting that the extrinsic pathway of apoptosis is involved at the later phase of ATP depletion.

Although it is understood that caspase-8 generally activates caspase-3, there is recent evidence of cross talk between the extrinsic and mitochondrial pathways of apoptosis. In fact it has been shown that caspase-8 activation by ROS formed during hypoxia–reoxygenation results in Bid cleavage and Bax activation, suggesting that the mitochondrial pathway is involved in caspase-8 mediated apoptosis [56]. Similarly, in this study, we found that although FeT-MPyP decreased the expression of the anti-apoptotic protein Bcl-2 slightly, it completely blocked the activation of pro-apoptotic protein, Bax, at the later time point of injury. In this regard, there is a recent report in a mouse model of spinal cord injury in which a related peroxynitrite decomposition catalyst, FeTSPP also blocks Bax activation [57] thereby preventing apoptosis. Thus, peroxynitrite mediated Bax activation and subsequent translocation to the mitochondria [58,59] may be a critical step for the release of cytochrome *c* from the mitochondria and downstream activation of caspase-9. Although we have not directly tested the effect of FeTMPyP on cytochrome *c* release in this study, we have previously shown that superoxide promotes the release of mitochondrial cytochrome *c* following ATP depletion-recovery [27]. It is therefore likely that peroxynitrite is playing a similar role in the activation of the mitochondrial pathway of apoptosis in this model of injury.

Conclusion

In conclusion, in this paper we have shown for the first time that FeTMPyP has a biphasic effect on apoptosis following ATP depletion-recovery in proximal tubular epithelial cells. At the early time points of injury, FeTMPyP directly inhibits NO and blocks caspase-3 activation, whereas at the later time points of injury, FeTMPyP may act by inhibition of FasL/TNF-α, caspase-8 and Bax gene expression. These data show that peroxynitrite induces apoptosis by activation of multiple pathways dependant on length and severity of insult following ATP depletion-recovery.

Acknowledgements

Supported in part by divisional funds and Pilot and Feasibility grant (NIH) to V. Nilakantan.

Abbreviations

ATP
: Adenosine triphosphate

FADD
: Fas associated death domain

FeTMPyP
: 5,10,15,20-tetrakis (2,4′5′-trimethyl-3′5′-disulphonatophenyl)5^{+}

HE
: Hydroethidine

IM
: Injury media

IR
: Ischemia-reperfusion

LLC-PK_1
: Porcine renal proximal tubular epithelial cells

MnSOD
: Manganese superoxide dismutase

MnTMPyP
: Manganese (III)tetrakis(1-methyl-4-pyridyl) porphyrin pentachloride

NO
: Nitric oxide

$O_2^{\bullet -}$
: Superoxide

PARP
: Poly-ADP-ribosyl synthetase

ROS
: Reactive oxygen species

TRADD
: TNFR1 associated death domain

References

1. Dagher PC. Modeling ischemia in vitro: selective depletion of adenine and guanine nucleotide pools. Am J Physiol Cell Physiol 2000;279:C1270–1277. [PubMed: 11003607]
2. Edelstein CL, Ling H, Schrier RW. The nature of renal cell injury. Kidney Int 1997;51:1341–1351. [PubMed: 9150442]
3. Lee YJ, Park SH, Jeung TO, et al. Effect of adenosine triphosphate on phosphate uptake in renal proximal tubule cells: involvement of PKC and p38 MAPK. J Cell Physiol 2005;205:68–76. [PubMed: 15880445]
4. Yu L, Gengaro PE, Niederberger M, Burke TJ, Schrier RW. Nitric oxide: a mediator in rat tubular hypoxia/reoxygenation injury. Proc Natl Acad Sci USA 1994;91:1691–1695. [PubMed: 7510405]
5. Beckman JS. Protein tyrosine nitration and peroxynitrite. Faseb J 2002;16:1144. [PubMed: 12087072]
6. Beckman JS, Chen J, Ischiropoulos H, Crow JP. Oxidative chemistry of peroxynitrite. Methods Enzymol 1994;233:229–240. [PubMed: 8015460]
7. Beckman JS, Ischiropoulos H, Zhu L, et al. Kinetics of superoxide dismutase- and iron-catalyzed nitration of phenolics by peroxynitrite. Arch Biochem Biophys 1992;298:438–445. [PubMed: 1416975]
8. Alvarez MN, Piacenza L, Irigoin F, Peluffo G, Radi R. Macrophage-derived peroxynitrite diffusion and toxicity to Trypanosoma cruzi. Arch Biochem Biophys 2004;432:222–232. [PubMed: 15542061]
9. Cruthirds DL, Novak L, Akhi KM, et al. Mitochondrial targets of oxidative stress during renal ischemia/reperfusion. Arch Biochem Biophys 2003;412:27–33. [PubMed: 12646264]
10. Ischiropoulos H, al-Mehdi AB. Peroxynitrite-mediated oxidative protein modifications. FEBS Lett 1995;364:279–282. [PubMed: 7758583]
11. Nilakantan V, Halligan NL, Nguyen TK, et al. Post-translational modification of manganese superoxide dismutase in acutely rejecting cardiac transplants: role of inducible nitric oxide synthase. J Heart Lung Transplant 2005;24:1591–1599. [PubMed: 16210135]
12. Quijano C, Alvarez B, Gatti RM, Augusto O, Radi R. Pathways of peroxynitrite oxidation of thiol groups. Biochem J 1997;322(Pt 1):167–173. [PubMed: 9078258]
13. Gow AJ, Farkouh CR, Munson DA, Posencheg MA, Ischiropoulos H. Biological significance of nitric oxide-mediated protein modifications. Am J Physiol Lung Cell Mol Physiol 2004;287:L262–L268. [PubMed: 15246980]
14. Gow AJ, Ischiropoulos H. Nitric oxide chemistry and cellular signaling. J Cell Physiol 2001;187:277–282. [PubMed: 11319751]
15. Greenacre SA, Ischiropoulos H. Tyrosine nitration: localisation, quantification, consequences for protein function and signal transduction. Free Radic Res 2001;34:541–581. [PubMed: 11697033]
16. Souza JM, Choi I, Chen Q, et al. Proteolytic degradation of tyrosine nitrated proteins. Arch Biochem Biophys 2000;380:360–366. [PubMed: 10933892]
17. Lorch S, Lightfoot R, Ohshima H, et al. Detection of peroxynitrite-induced protein and DNA modifications. Methods Mol Biol 2002;196:247–275. [PubMed: 12152205]
18. Niles JC, Wishnok JS, Tannenbaum SR. Peroxynitrite-induced oxidation and nitration products of guanine and 8-oxoguanine: structures and mechanisms of product formation. Nitric Oxide 2006;14:109–121. [PubMed: 16352449]
19. Cruthirds DL, Saba H, MacMillan-Crow LA. Overexpression of manganese superoxide dismutase protects against ATP depletion-mediated cell death of proximal tubule cells. Arch Biochem Biophys 2005;437:96–105. [PubMed: 15820221]
20. Khand FD, Gordge MP, Robertson WG, Noronha-Dutra AA, Hothersall JS. Mitochondrial superoxide production during oxalate-mediated oxidative stress in renal epithelial cells. Free Radic Biol Med 2002;32:1339–1350. [PubMed: 12057772]
21. Kim YK, Lee SK, Ha MS, Woo JS, Jung JS. Differential role of reactive oxygen species in chemical hypoxia-induced cell injury in opossum kidney cells and rabbit renal cortical slices. Exp Nephrol 2002;10:275–284. [PubMed: 12097831]
22. Hagar H, Ueda N, Shah SV. Role of reactive oxygen metabolites in DNA damage and cell death in chemical hypoxic injury to LLC-PK_1 cells. Am J Physiol 1996;271:F209–F215. [PubMed: 8760263]

23. Butterfield DA, Boyd-Kimball D, Castegna A. Proteomics in Alzheimer's disease: insights into potential mechanisms of neurodegeneration. J Neurochem 2003;86:1313–1327. [PubMed: 12950441]
24. Lieberthal W, Levine JS. Mechanisms of apoptosis and its potential role in renal tubular epithelial cell injury. Am J Physiol 1996;271:F477–F488. [PubMed: 8853409]
25. Lieberthal W, Menza SA, Levine JS. Graded ATP depletion can cause necrosis or apoptosis of cultured mouse proximal tubular cells. Am J Physiol 1998;274:F315–F327. [PubMed: 9486226]
26. Bagnasco S, Good D, Balaban R, Burg M. Lactate production in isolated segments of the rat nephron. Am J Physiol 1985;248:F522–F526. [PubMed: 3985159]
27. Maenpaa CJ, Shames BD, Van Why SK, Johnson CP, Nilakantan V. Oxidant-mediated apoptosis in proximal tubular epithelial cells following ATP depletion and recovery. Free Radic Biol Med 2008;44:518–526. [PubMed: 17997382]
28. Borutaite V, Brown GC. Rapid reduction of nitric oxide by mitochondria, and reversible inhibition of mitochondrial respiration by nitric oxide. Biochem J 1996;315(Pt 1):295–299. [PubMed: 8670121]
29. Brown GC, Borutaite V. Inhibition of mitochondrial respiratory complex I by nitric oxide, peroxynitrite and S-nitrosothiols. Biochim Biophys Acta 2004;1658:44–49. [PubMed: 15282173]
30. Batthyany C, Souza JM, Duran R, et al. Time course and site(s) of cytochrome c tyrosine nitration by peroxynitrite. Biochemistry 2005;44:8038–8046. [PubMed: 15924423]
31. Cassina AM, Hodara R, Souza JM, et al. Cytochrome c nitration by peroxynitrite. J Biol Chem 2000;275:21409–21415. [PubMed: 10770952]
32. Szabo C, Zingarelli B, O'Connor M, Salzman AL. DNA strand breakage, activation of poly (ADP-ribose) synthetase, and cellular energy depletion are involved in the cytotoxicity of macrophages and smooth muscle cells exposed to peroxynitrite. Proc Natl Acad Sci U S A 1996;93:1753–1758. [PubMed: 8700830]
33. Lancel S, Tissier S, Mordon S, et al. Peroxynitrite decomposition catalysts prevent myocardial dysfunction and inflammation in endotoxemic rats. J Am Coll Cardiol 2004;43:2348–2358. [PubMed: 15193704]
34. Salvemini D, Wang ZQ, Stern MK, Currie MG, Misko TP. Peroxynitrite decomposition catalysts: therapeutics for peroxynitrite-mediated pathology. Proc Natl Acad Sci U S A 1998;95:2659–2663. [PubMed: 9482943]
35. Cuzzocrea S, Misko TP, Costantino G, et al. Beneficial effects of peroxynitrite decomposition catalyst in a rat model of splanchnic artery occlusion and reperfusion. Faseb J 2000;14:1061–1072. [PubMed: 10834927]
36. Dhar A, Kaundal RK, Sharma SS. Neuroprotective effects of FeTMPyP: a peroxynitrite decomposition catalyst in global cerebral ischemia model in gerbils. Pharmacol Res 2006;54:311–316. [PubMed: 16877004]
37. Stefanutti G, Pierro A, Smith VV, Klein NJ, Eaton S. Peroxynitrite decomposition catalyst FeTMPyP provides partial protection against intestinal ischemia and reperfusion injury in infant rats. Pediatr Res 2007;62:43–48. [PubMed: 17515836]
38. Wang XL, Liu HR, Tao L, et al. Role of iNOS-derived reactive nitrogen species and resultant nitrative stress in leukocytes-induced cardiomyocyte apoptosis after myocardial ischemia/reperfusion. Apoptosis 2007;12:1209–1217. [PubMed: 17333318]
39. Khadour FH, Panas D, Ferdinandy P, et al. Enhanced NO and superoxide generation in dysfunctional hearts from endotoxemic rats. Am J Physiol Heart Circ Physiol 2002;283:H1108–H1115. [PubMed: 12181141]
40. Nilakantan V, Zhou X, Hilton G, et al. Hierarchical change in antioxidant enzyme gene expression and activity in acute cardiac rejection: role of inducible nitric oxide synthase. Mol Cell Biochem 2005;270:39–47. [PubMed: 15792352]
41. van Why SK, Kim S, Geibel J, et al. Thresholds for cellular disruption and activation of the stress response in renal epithelia. Am J Physiol 1999;277:F227–F234. [PubMed: 10444577]
42. Beckman JS, Beckman TW, Chen J, Marshall PA, Freeman BA. Apparent hydroxyl radical production by peroxynitrite: implications for endothelial injury from nitric oxide and superoxide. Proc Natl Acad Sci U S A 1990;87:1620–1624. [PubMed: 2154753]

43. Radi R. Nitric oxide, oxidants, and protein tyrosine nitration. Proc Natl Acad Sci U S A 2004;101:4003–4008. [PubMed: 15020765]
44. Radi R, Peluffo G, Alvarez MN, Naviliat M, Cayota A. Unraveling peroxynitrite formation in biological systems. Free Radic Biol Med 2001;30:463–488. [PubMed: 11182518]
45. Kang JL, Lee HS, Pack IS, Leonard S, Castranova V. Iron tetrakis (n-methyl-4′-pyridyl) porphyrinato (FeTMPyP) is a potent scavenging antioxidant and an inhibitor of stimulant-induced NF-kappaB activation of raw 264.7 macrophages. J Toxicol Environ Health A 2001;64:291–310. [PubMed: 11693489]
46. Tiwari MM, Messer KJ, Mayeux PR. Inducible nitric oxide synthase and apoptosis in murine proximal tubule epithelial cells. Toxicol Sci 2006;91:493–500. [PubMed: 16551643]
47. Chien CT, Hsu SM, Chen CF, Lee PH, Lai MK. Prolonged ischemia potentiates apoptosis formation during reperfusion by increase of caspase 3 activity and free radical generation. Transplant Proc 2000;32:2065–2066. [PubMed: 11120068]
48. Chien CT, Lee PH, Chen CF, et al. De novo demonstration and co-localization of free-radical production and apoptosis formation in rat kidney subjected to ischemia/reperfusion. J Am Soc Nephrol 2001;12:973–982. [PubMed: 11316856]
49. Faubel S, Edelstein CL. Caspases as drug targets in ischemic organ injury. Curr Drug Targets Immune Endocr Metabol Disord 2005;5:269–287. [PubMed: 16178788]
50. Jang M, Park BC, Lee AY, et al. Caspase-7 mediated cleavage of proteasome subunits during apoptosis. Biochem Biophys Res Commun 2007;363:388–394. [PubMed: 17880920]
51. Hortelano S, Castilla M, Torres AM, Tejedor A, Bosca L. Potentiation by nitric oxide of cyclosporin A and FK506-induced apoptosis in renal proximal tubule cells. J Am Soc Nephrol 2000;11:2315–2323. [PubMed: 11095654]
52. Wang MJ, Liu S, Liu Y, Zheng D. Actinomycin D enhances TRAIL-induced caspase-dependent and -independent apoptosis in SH-SY5Y neuroblastoma cells. Neurosci Res 2007;59:40–46. [PubMed: 17707539]
53. Chinnaiyan AM, Dixit VM. The cell-death machine. Curr Biol 1996;6:555–562. [PubMed: 8805273]
54. Chinnaiyan AM, O'Rourke K, Tewari M, Dixit VM. FADD, a novel death domain-containing protein, interacts with the death domain of Fas and initiates apoptosis. Cell 1995;81:505–512. [PubMed: 7538907]
55. Nagata S. Apoptosis by death factor. Cell 1997;88:355–365. [PubMed: 9039262]
56. Kim BM, Chung HW. Hypoxia/reoxygenation induces apoptosis through a ROS-mediated caspase-8/Bid/Bax pathway in human lymphocytes. Biochem Biophys Res Commun 2007;363:745–750. [PubMed: 17904098]
57. Genovese T, Mazzon E, Esposito E, et al. Beneficial effects of FeTSPP, a peroxynitrite decomposition catalyst, in a mouse model of spinal cord injury. Free Radic Biol Med 2007;43:763–780. [PubMed: 17664140]
58. Shacka JJ, Sahawneh MA, Gonzalez JD, et al. Two distinct signaling pathways regulate peroxynitrite-induced apoptosis in PC12 cells. Cell Death Differ 2006;13:1506–1514. [PubMed: 16410804]
59. Capano M, Crompton M. Biphasic translocation of Bax to mitochondria. Biochem J 2002;367:169–178. [PubMed: 12097139]

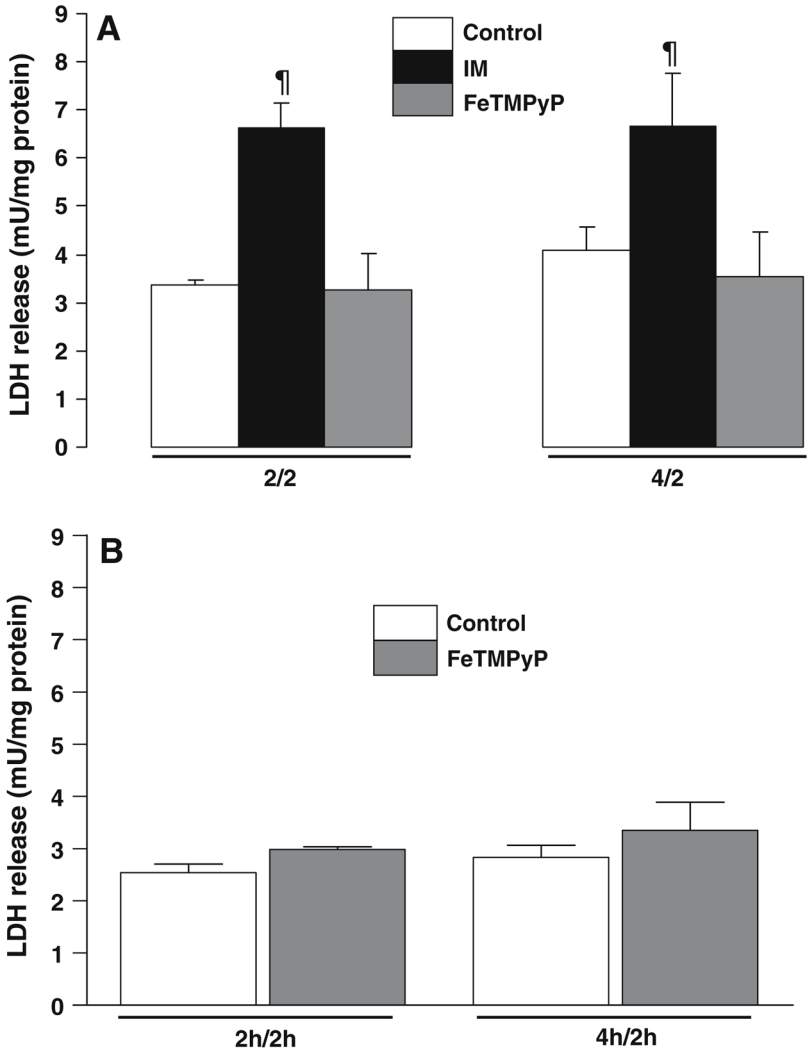

Fig. 1.

Effect of FeTMPyP on cytotoxicity in LLC-Pk$_1$ cells following ATP depletion-recovery. (a) LDH release was measured in media following 2 h or 4 h ATP depletion with 2 h recovery (designated as 2/2, 4/2) of the LLC-PK$_1$ cells. Groups include serum free control cells (Control), injured cells (IM) and FeTMPyP treated injured cells (100 μM, FeTMPyP). Results are means ± SEM (n = 3–9 for all groups). $^{¶}P < 0.01$ IM vs. control and FeTMPyP. (b) LDH release was measured in the media following either 4 (2/2 time point) or 6 h (4/2 time point) incubation with 100 μM FeTMPyP. Groups include serum free control cells (Control) and FeTMPyP treated cells (FeTMPyP). Results are means ± SEM (n = 3 for all groups)

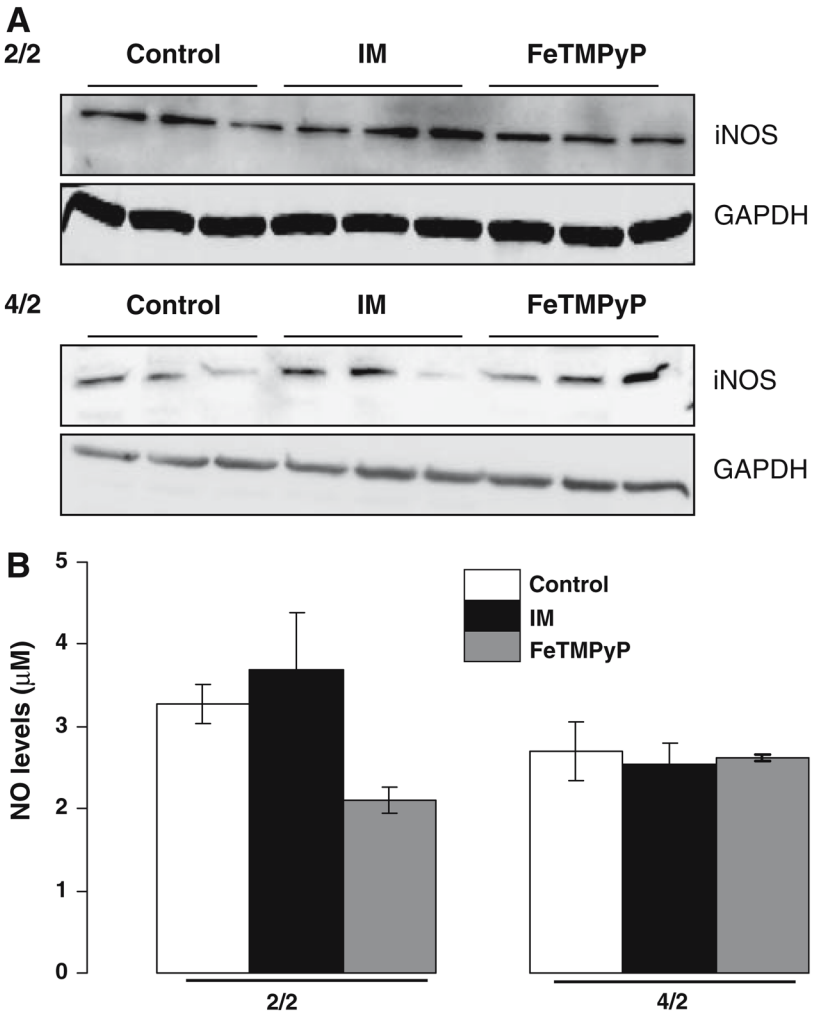

Fig. 2.

Effect of FeTMPyP on NO in LLC-Pk$_1$ cells following ATP depletion-recovery. (a) Western Blotting showing iNOS protein levels in serum free (Control), ATP depleted (IM) and FeTMPyP (FeT-MPyP) treated cells following 2 h ATP depletion-2 h recovery (2/2, top panel) and 4 h ATP depletion-2 h recovery (4/2, bottom panel). (b) NO levels as measured by the NO analyzer in the media of LLC-PK$_1$ cells following ATP depletion for either 2 h or 4 h (designated as 2/2 and 4/2) followed by 2 h recovery in serum free media. Groups include serum free control cells (Control), injured cells (IM) and FeTMPyP treated injured cells (100 μM, FeTMPyP). Results are means ± SEM (n = 4–9 for all groups). Results not significantly different from each other

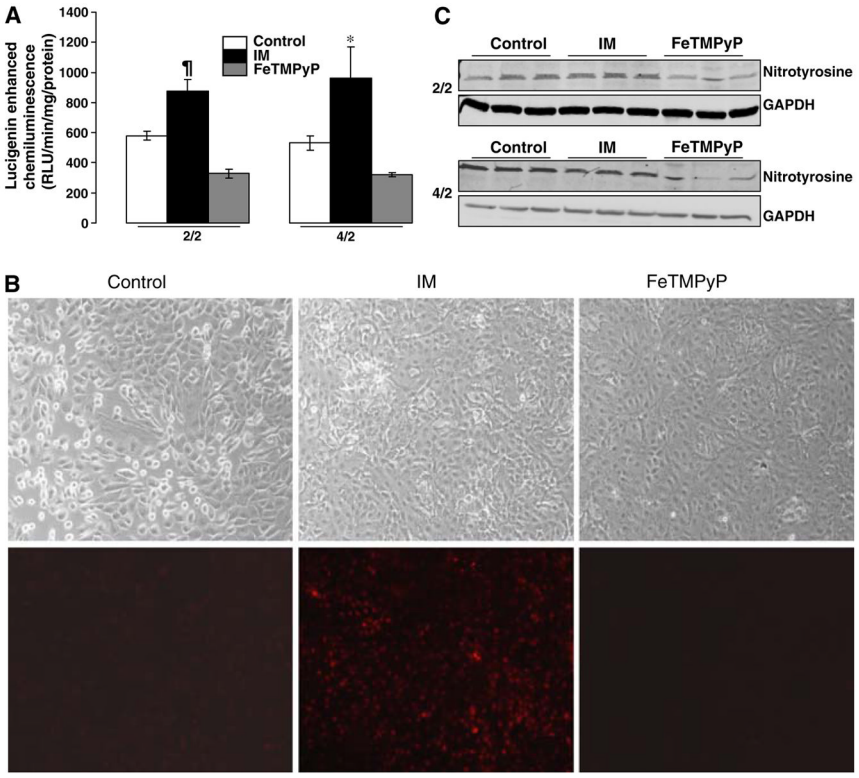

Fig. 3.

Effect of FeTMPyP on ROS in LLC-PK$_1$ cells following ATP depletion-recovery. (a) ROS levels as measured by lucigenin enhanced chemiluminescence in LLC-PK$_1$ cells following ATP depletion for either 2 h or 4 h (designated as 2/2 and 4/2) followed by recovery in serum free media for 2 h. Groups include serum free control cells (Control), injured cells (IM) and FeTMPyP treated injured cells (100 μM, FeTMPyP). Results are means ± SEM (n = 4–6 for 2/2 and n = 3 for 4/2). ¶$P < 0.01$ IM vs. control and FeTMPyP, *$P < 0.05$ IM vs. control and FeTMPyP. (b) DHE fluorescent microscopic images (10x), used to identify ROS in serum free control cells (Control), injured cells at time point 2/2 (IM), and injury with FeTMPyP (100 μM, FeTMPyP). ATP depletion-recovery at time point 2/2 resulted in increased DHE fluorescence (lower panels); FeTMPyP blocked DHE fluorescence completely (lower panels). Light microscopic images of the same fields are shown in the upper panels. Three separate cultures from each group were analyzed and a representative image is shown. (c) Western Blotting showing nitrotyrosine levels in serum free (control), ATP depleted (IM) and FeTMPyP treated LLC-Pk1 cells following 2 h ATP depletion-2 h recovery (2/2 time point) and 4 h ATP depletion-2 h recovery (4/2 time point)

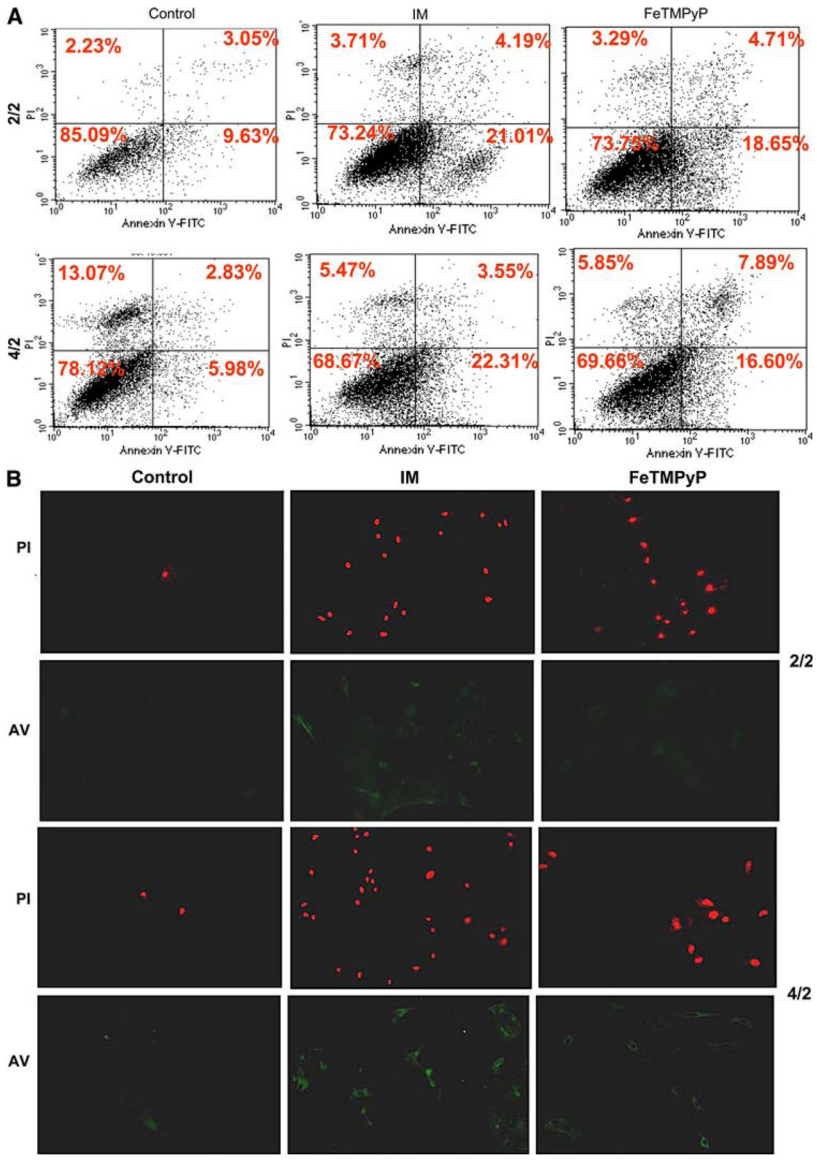

Fig. 4.

(a) Flow cytometry of AnnexinV/Propidium Iodide stained LLC-Pk_1 cells following ATP depletion-recovery showing an increase in early apoptotic signaling in injured cells (IM) vs. serum free (control) and FeTMPyP treated (FeTMPyP) cells at time points 2/2 and 4/2. (b) Microscopic images of Propidium Iodide (red staining, top panels for 2/2 and 4/2 respectively) and Annexin V (green staining, bottom panels of 2/2 and 4/2 respectively) in serum free (control), ATP depleted (IM) and FeTMPyP treated cells following ATP depletion-recovery at the 2/2 and 4/2 time points

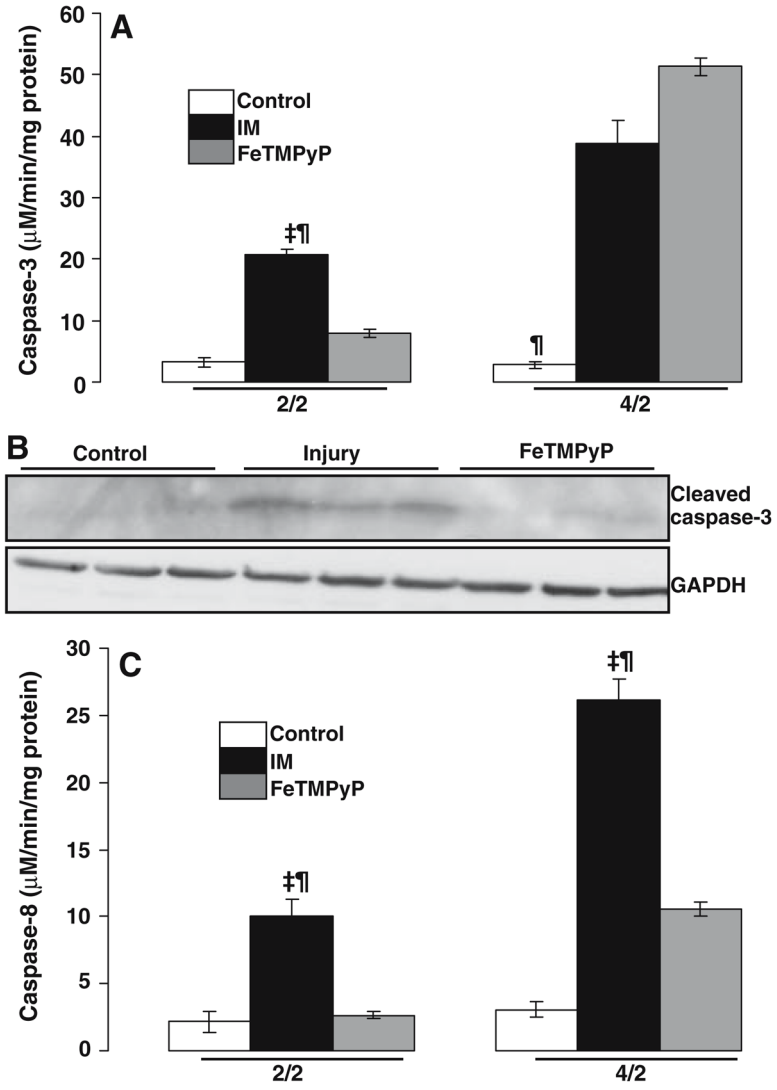

Fig. 5.

Effect of FeTMPyP on caspase activity in LLC-Pk$_1$ cells following ATP depletion-recovery. (a) Effect of FeTMPyP on caspase-3 activation following ATP depletion for either 2 h or 4 h (designated as 2/2 and 4/2) followed by recovery in serum free media for 2 h. Groups include serum free control cells (Control), injured cells (IM) and FeTMPyP treated injured cells (100 μM, FeTMPyP). Results are means ± SEM (n = 3 for all groups). For 2/2, $^{‡}P < 0.001$ IM vs. serum free, $^{¶}P < 0.01$ IM vs. FeTMPyP; for 4/2 $^{¶}P < 0.01$ control vs. IM and FeTMPyP. (b) Western Blotting showing effect of FeTMPyP on cleaved caspase-3 in serum free (control), ATP depleted (IM) and FeTMPyP treated samples at the 4/2 time point. (c) Effect of FeTMPyP on casaspe-8 activation following ATP depletion for either 2 h or 4 h (designated as 2/2 and 4/2) followed by recovery in serum free media for 2 h. Groups include serum free control cells (Control), injured cells (IM) and FeTMPyP treated injured cells (100 μM, FeTMPyP). Results are means ± SEM (n = 3 for all groups). $^{‡}P < 0.001$ IM vs. control, $^{¶}P < 0.01$ IM vs. FeTMPyP

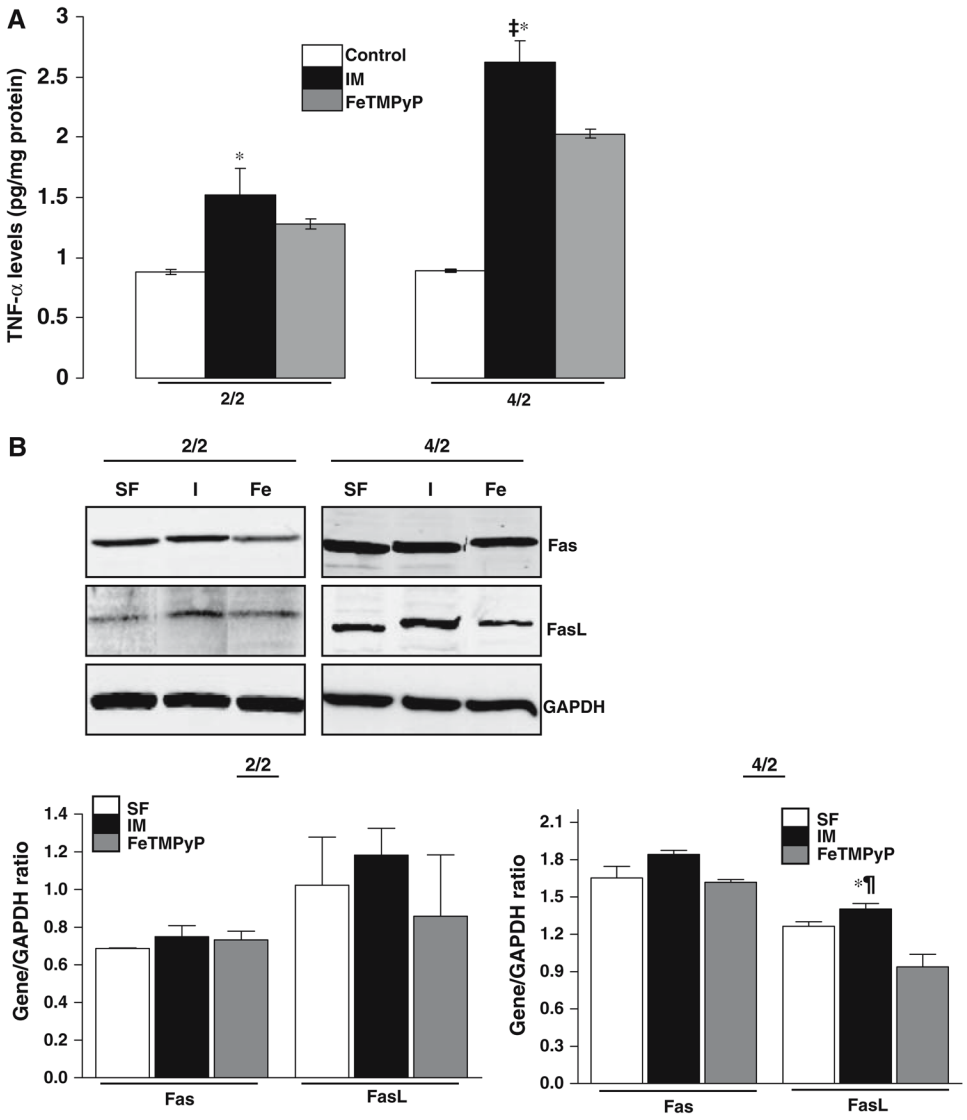

Fig. 6.

Effect of FeTMPyP on the extrinsic pathway of apoptosis in LLC-PK$_1$ cells following ATP depletion-recovery. (a) TNF-α levels in LLC-PK$_1$ cells following ATP depletion for either 2 h or 4 h (designated as 2/2 and 4/2) followed by recovery in serum free media for 2 h. Groups include serum free control cells (Control), injured cells (IM) and FeTMPyP treated injured cells (100 μM, FeTMPyP). Results are means ± SEM ($n = 3$ for all groups). For 2/2, *$P < 0.05$ IM vs. control; for 4/2, ‡$P < 0.001$ IM vs. control, *$P < 0.05$ IM vs. FeTMPyP. (b) Effect of FeTMPyP on Fas and FasL expression in serum free control (C), injured (I) and FeTMPyP treated (Fe) cells following 2 h ATP dpeletion-2 h recovery (2/2, left panel) and 4 h ATP depletion-2 h recovery (4/2, right panel). The bottom image depicts the densitometry for normalized gene/GAPDH ratio for time points 2/2 (left panel) and 4/2 (right panel) respectively

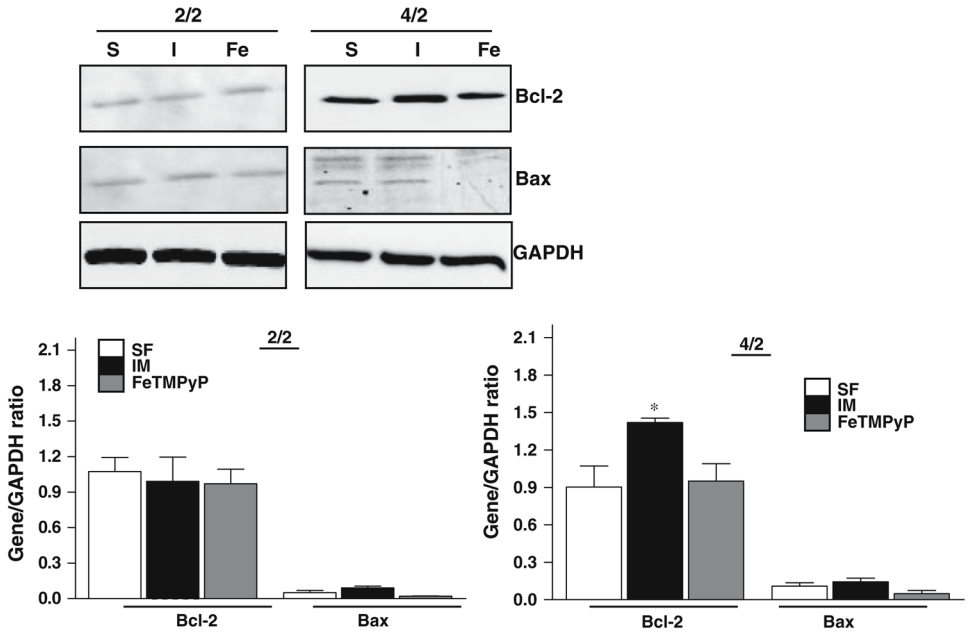

Fig. 7.

Effect of FeTMPyP on Bcl-2 and Bax expression in serum free control (C), injured (I) and FeTMPyP treated (Fe) cells following 2 h ATP dpeletion-2 h recovery (2/2, left panel) and 4 h ATP depletion-2 h recovery (4/2, right panel). The bottom image depicts the densitometry for normalized gene/GAPDH ratio for time points 2/2 (left panel) and 4/2 (right panel) respectively